

NATIONAL AERONAUTICS AND SPACE ADMINISTRATION

TECHNICAL MEMORANDUM X-607

LAUNCH-VEHICLE DYNAMICS\* \*\*

By Harry L. Runyan, Jr., and A. Gerald Rainey

SUMMARY

Structural-dynamics problems pertinent to the design of launch vehicles suitable for a lunar mission are discussed. Some measurements of the natural modes of a model of the Saturn launch vehicle are presented. Recent information concerning launch-vehicle loads associated with buffeting, aerodynamic noise, and winds is also presented.

INTRODUCTION

The idea that a launch vehicle is a space truck on which any spacecraft, within performance capabilities, can be carried without giving due consideration to problems of structural dynamics can lead and has led to serious consequences. A launch vehicle with a new spacecraft is in essence a new system. The purpose of this discussion is to present several of the more important factors affecting launch-vehicle dynamics both with regard to system inputs and dynamic behavior.


SYMBOLS

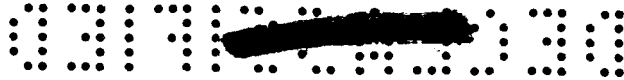
$C$	damping
$C_{cr}$	critical damping
$\Delta C_{p,rms}$	root mean square of incremental pressure coefficient
$f_{exp}$	experimental frequency, cps
$f_{cal}$	calculated frequency, cps

---

\*This report was one of the papers presented at the NASA-Industry Apollo Conference, Washington, D.C., July 18-20, 1961.

\*\*Title, Unclassified.





$M_b$  bending moment, in-lb

$M_\infty$  free-stream Mach number

$q$  dynamic pressure, lb/sq ft

### LAUNCH-VEHICLE LOADING INPUTS

In figure 1 are listed some of the more important loading inputs plotted against time of flight; namely, lift-off, transonic effects, and maximum dynamic pressure. The dark areas represent the times of maximum loading for the particular source. Indicated are such load sources as fuel slosh, acoustics, buffet, panel flutter, and winds. The main purpose of this figure is to illustrate that most of the loads occur between the vertical lines which indicate the transonic and maximum dynamic-pressure conditions. Most of the loads are shown to reach a maximum value at about the same time during the flight. Briefly discussed are some details concerning ground wind loads, acoustics, buffet, and winds, as well as the vibration modes, which in effect comprise the transfer function for buffet, fuel slosh, and wind loads of Saturn.

L  
1  
7  
5  
5

### SATURN VIBRATION CHARACTERISTICS

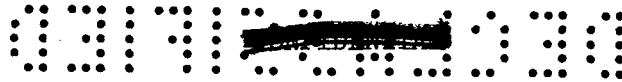
One of the basic ingredients in the design of a control system and in loads estimation is an accurate knowledge of the launch-vehicle vibration characteristics. Both the vibration mode shapes and the frequencies must be known to ensure that no coupling will exist between the control-system sensors and the structural modes. The Saturn is the launch vehicle for the Apollo program; therefore, an accurate knowledge of the vibration characteristics is needed as early as possible. A 1/5-scale dynamic model of the Saturn has been constructed for investigation at the Langley Research Center. Figure 2 illustrates the model installed in the test tower. (The man shown indicates in general the size of the model.) The model is suspended by an unusual and simple system which provides very little restraint from the support system and thus approximates a free-free system such as occurs in flight. The comparatively large model scale (1/5) was chosen to permit accurate simulation of joints, fittings, and skin gages, which were considered especially important for the cluster configuration, since motion of tanks within the cluster relative to each other is possible. This model program can also provide immediate modal and frequency data for the Saturn program, demonstrate the feasibility of obtaining accurate vibration data from scaled models, and provide a test bed to evaluate future changes in the vehicle, along with future payloads.



Free-free vibration tests of the model have been made, and data have been obtained with the model ballasted with water to simulate the weight at the point of maximum dynamic pressure in the launch trajectory. Figure 3 shows the acceleration response of a point on the nose of the vehicle for various driving frequencies. The frequencies have been scaled to correspond to full-scale frequencies. The driving force was provided by two electromagnetic shakers, located at the top and bottom of the model. The large number of peaks that appear indicate a number of resonant frequencies. For comparison purposes, the arrows have been placed on the abscissa to show natural frequencies calculated by simple beam theory, which assumes an equivalent stiffness for the clustered-tank portion of the launch vehicle. Notice that the calculated frequencies agree fairly well with some of the measured peaks. It is apparent, also, that several frequencies appear experimentally which were not predicted analytically. These results indicate additional vibration modes or effects in the model not accounted for by the simple analysis. The predominant characteristic of these higher modes (and their frequencies are still low enough to be of concern in control-system design) is the large amount of relative motion between the various tanks in the booster cluster. This phenomenon is illustrated by the measured mode shapes which correspond to the two lowest frequencies of the model.

The measured mode shape corresponding to the first resonant peak is shown in figure 4. The deflection of the center line is plotted, normalized to unit deflection at the nose of the launch vehicle. The calculated first mode is also plotted (as a dashed line) and indicates good agreement with the experiment. The behavior of the cluster is shown in the cross-section A-A. The arrows indicate the relative motion of each tank. Note that all tanks move together, with about the same amplitude. The overall behavior observed for this mode is that of bending as a beam, predictable by the usual methods of vibration analysis.

The behavior is considerably different when the experimental vibration mode corresponding to the second resonant frequency is examined (fig. 5). The center-line deflection, plotted in the center, now shows only one node point, in contrast to three node points expected from beam behavior. The predicted mode shape, obtained by the beam analogy, is sketched as a dashed line to show this deviation. Again, the arrows are used to indicate the relative motion of individual tanks (section A-A). If the center tank moves in one direction, the tanks on the sides move directly opposite. The tanks in line with the motion of the center body tend to remain still, while the remaining four tanks actually have a component of motion out of the plane of the exciting force. However, these tanks still tend to move opposite to the center tank. The mode of one of these tanks on the sides has been superimposed on the center-line mode, in the middle sketch, to show the



relative amplitude of the tank motion. Note that the tank motion is relatively larger than the center-line motion. Because of the rather complicated motion of this mode, it has been termed a "cluster" mode, rather than a second beam bending mode as it would be in the conventional case. The other resonant peaks shown on the frequency response curve have equally complicated modal patterns, containing not only relative motion of tanks within the cluster but also local distortions and shell-type responses.

Vibration tests on the model are continuing in order to better define and understand the vibration characteristics of the Saturn and for extension to future clustered configurations. A full-scale vibration test is being conducted at Marshall Space Flight Center, and correlation of model and full-scale test results is planned in order to demonstrate the feasibility and accuracy of model test results. More refined analyses of vibration characteristics will also be necessary in order to develop and prove the analytical techniques.


It is anticipated that the model will be kept up-to-date so that later configurations including, for instance, a dynamically scaled Apollo spacecraft, may be tested.

#### GROUND-WIND EFFECTS

The next subject to be discussed concerns the loads caused by the ground winds on the launch vehicle while supported on the launch stand. The loads resulting from steady winds manifest themselves in two ways. First, there exists a drag load and, consequently, a steady bending moment in the direction of the winds. The second loading manifests itself in an oscillation, principally in the direction normal to the wind. Data obtained on a dynamic model of Saturn (fig. 6) tested in the Langley transonic dynamics tunnel are shown in figure 7.

In this investigation, the response of a dynamically and elastically scaled 1/13-scale model of the Saturn SA-1 vehicle was measured at simulated ground winds up to 80 feet per second and at full-scale Reynolds numbers. The model results shown have been scaled up to the full-size Saturn. For the data presented, the model airstream orientation was such that one of the eight barrels along the launch vehicle was directly in line with the wind.

In figure 7 the steady-drag bending moment measured at the base tie-down location (station 121.75) is presented; also presented, for comparison, is the maximum oscillatory bending moment in the lateral (perpendicular to the wind) direction, which was the largest oscillatory bending moment measured. At low velocities the oscillatory



SECRET

5

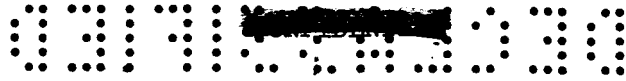
bending moment generally exceeds the steady-drag bending moment. At higher velocities the steady-drag moment becomes several times the oscillatory moment and approaches the static overturn moment for the unfueled vehicle resting unclamped on the launch arms. Thus, for the Saturn SA-1 the critical load from ground winds is the steady-drag load rather than the oscillatory response lateral to the winds, which has been the critical load for some other launch vehicles.

The variation with wind velocity of the maximum oscillatory base bending moments in the drag direction has also been obtained. As is typical of such cylindrical structures, the oscillatory response in the lateral direction was much greater than in the drag direction. Of general interest is the unexpected peak in the response at velocities of about 30 feet per second, which are not typical of supercritical Reynolds number responses. Adding roughness or spoilers to the nose of the model increased the peak response at this velocity. Other data indicate that the peak tends to disappear if the plain model is rotated  $22.5^\circ$  to orient the valley between two barrels to a position aligned with the wind direction. Therefore, it may be that this peak response is a function of the details of the flow around the eight barrels of the launch vehicle which present a noncylindrical shape to the airstream. It seems unlikely that this peak response at low wind velocities will present a problem to the Saturn SA-1 since, as is shown in figure 7, the steady-drag moment at higher wind velocities is much greater than this peak oscillatory moment.

#### AERODYNAMIC NOISE

The next subject to be considered is the noise environment of the vehicle, both at launch and during flight. The two main sources of noise for the Saturn launched Apollo vehicle will be the rocket engines and the aerodynamic boundary layer. In figure 8 the estimated noise levels outside the manned region of a two-stage Apollo vehicle are shown as a function of time. The noise levels from the rocket engines and from the aerodynamic boundary layer are indicated by the cross-hatched area and single-hatched areas, respectively. The rocket-engine noise levels are based on measured data obtained for Saturn static firings and Atlas launching tests. The highest rocket-engine noise levels are indicated during the static firing and lift-off because of flow impingement and ground reflections. After the vehicle leaves the ground, there is a decrease in the rocket-engine noise levels because of beneficial effects of the vehicle forward velocity. The aerodynamic noise levels increase as the dynamic pressure increases, the noise pressures being approximately proportional to the dynamic pressure. The aerodynamic noise levels shown are based on estimated

SECRET



dynamic pressures for the Apollo spacecraft. The extent of the cross-hatched areas is based on wind-tunnel studies and flight data for aircraft and for Project Mercury spacecraft; the lower limit applies to clean aerodynamic surfaces ( $0.006q$ ), whereas the upper limit is for regions of separated flow ( $0.02q$ ).


It should be noted that the estimated noise levels are for a region of the vehicle where the manned compartment might be located. For regions of the vehicle near the rocket-engine nozzles, noise levels approximately 15 db higher than those on the nose would be expected during static firing and lift-off. The aerodynamic noise levels estimated are believed to be of about the same order of magnitude for other regions of the vehicle; however, there would probably be differences in the spectral content of the noise (i.e., the peak of the spectrum would shift toward lower frequencies for regions farther aft).

#### BUFFETING

Buffeting of launch vehicles is a relatively new problem which has received considerable attention in the past year. This buffeting has been suspected as a cause for several vehicle failures, either directly through structural failures or indirectly because of failure of equipment subjected to the severe environment produced by buffeting flows.

Buffeting occurs on a wide variety of aerodynamic shapes. Some of the configurations which are representative of those used in various NASA research programs are shown in figure 9. The so-called "hammerhead" shapes which are used as payload fairings on several vehicles are very susceptible to buffeting flows at transonic speeds. The cone-cylinder-flare configurations used on several warhead reentry vehicles are also subject to buffeting. And, of course, the configurations with escape towers, such as Mercury and some Apollo configurations, also have their buffeting problems. These and other shapes are under intensive investigation.

The three different types of shapes produce at least three different types of buffeting flow, which are illustrated schematically in figure 10. The first type of flow is very similar to the familiar transonic buffeting of thick airfoils. At Mach numbers just below 1.0 the flow expands to supersonic speed over the thicker portion of the nose and is terminated by a normal shock, which in general separates the boundary layer in an unstable manner and produces large pressure fluctuations near the shock location. The second type of flow illustrated is associated with the separation caused by the high pressure, produced by the flare, propagating forward through the boundary layer.



SECRET

7

This type of flow can persist to low supersonic Mach numbers and is often intermittently asymmetrical even at zero angle of attack. The third type of flow resembles wake buffet in that it is similar to the flow phenomena of an airplane having its horizontal tail in or near the wake of the wing. Various types of protuberances on the forward part of the launch vehicle can produce a wake which passes back over the body of the vehicle and causes the shocks to fluctuate with large pressure fluctuations. This type of buffeting also persists to low supersonic speeds and can be a serious problem at the time of maximum dynamic pressure as well as near Mach number 1. Of course, this is just one particular listing of types of buffeting flows. Some configurations experience combinations of all these types and others as well.

An example of specific results obtained at Ames Research Center for one model (ref. 1) is shown in figure 11. The root-mean-square values of pressure coefficient are shown plotted against pressure cell location for a cone-cylinder combination similar to the Centaur launch vehicle. Results are shown for three subsonic Mach numbers. Of particular note is the highly localized characteristic of this type of buffet at each Mach number which occurs at or near the intersection of the cone and cylinder. However, this pressure peak shifts back with increasing Mach number, so that even though it is of a highly localized nature, strengthening of the structure may be required over a considerable length of the vehicle. Similar results have been obtained on essentially every configuration being flown in the space program as well as on a number of planned configurations.

In order to obtain an indication of the buffet characteristics of Apollo spacecraft during launch, a model of one of the Apollo design configurations has been tested in the Langley 8-foot transonic pressure tunnel. In figure 12 the fluctuating pressures in the form of a root-mean-square pressure coefficient are plotted at the various locations on the spacecraft and second stage. The pressure fluctuations on the nose are small for both configurations, but the presence of the tower causes very high pressure fluctuations over the downstream portions. This highest value just behind the shoulder of the spacecraft is about 23 percent of free-stream dynamic pressure on the basis of root-mean-square values. This effect would correspond to fluctuating peak pressures of nearly 430 pounds per square foot for a nominal Saturn launch trajectory.

This large effect of the escape tower differs from results obtained on the Mercury configuration, which indicated generally high levels (16 percent of  $q$ ) either with or without the tower. It is evident that more basic research will be required to obtain a full understanding of these phenomena. The limited amount of information obtained with this model indicates that a buffet problem can exist for Apollo. During the development of the vehicle, careful consideration should be given to the configuration modifications that might alleviate the problem, and detailed studies appear necessary to ensure that the structure, equipment, and occupants can perform under the buffeting environment.

SECRET

CONFIDENTIAL

As a final item in this buffet problem, recent wind-tunnel results obtained at the Ames Research Center indicated that for certain nose shapes (principally the hammerhead) the aerodynamic buffet forces are phased in such a manner that a condition of negative damping can occur in a vibration mode. This result means, simply, that a single-degree-of-freedom flutter is possible. At the Langley Research Center, a flexible model has been tested and the damping in the first elastic mode is shown in figure 13. The damping ratio is plotted against Mach number for two configurations. One represents a clean configuration and the damping (structural plus aerodynamic) is shown to be above the structural damping which is indicated by the dashed line. Thus, this configuration has positive damping and is stable. The second configuration, shown at the lower part of the figure, has a region of negative aerodynamic damping as shown by the region where it is below the structural-damping line. Thus, it is apparent that elastic models of proposed configurations should be tested to determine the possibility of negative aerodynamic damping.

L  
1  
7  
5  
5

#### WIND LOADS

The largest single source of loads on a launch vehicle during the atmospheric portion of the flight is due to the wind velocities normal to the launch-vehicle flight path. This problem of wind loads may be resolved into two parts. The first deals with the proper selection of the wind velocities to be used in the basic design, i.e., a design criterion. The second, of an operational nature, involves the requirement of a knowledge of the winds shortly before a firing so that a decision can be made with regard to the probability of success. As regards the design wind loads, the present practice utilizes an envelope of winds such that the winds over the altitude range of interest will not be exceeded for a certain percentage of time, which are referred to as 1, 2, or 3σ Sissenwine winds. These curves are essentially a series of straight lines and hence do not contain information concerning the details of the wind velocities. As a means of partially accounting for this neglected loading source, it is common practice to superimpose on the loading determined from the steady winds the loading determined from flying through a single 1 - cosine wind gust (which is tuned to excite the fundamental structural mode). The actual winds, of course, have a large number of wind variations which, coupled with low aerodynamic and structural damping, could excite the lower structural modes. An example of the finer grain structure of the winds is shown by the solid line in figure 14, where the altitude is plotted against wind velocity. Unfortunately, the large quantity of information needed to provide more precise wind criteria is lacking. A rather concentrated effort is being made, however, to determine the fine-grain structure of winds. At Langley Research Center, a smoke-trail technique (ref. 2) has been

CONFIDENTIAL



developed for obtaining more precise measurements of the winds. This technique utilizes either the natural exhaust of a solid-propellant rocket or an artificially generated smoke trail. Photographs are taken of the trail from two positions which are about ten miles from the launch site. From these photographs, then, the fine-grain detail of the wind velocities may be determined. The winds shown in figure 14 were obtained by the smoke-trail procedure, as well as by a simulated balloon sounding.

The simulated balloon sounding was obtained by reading and averaging the smoke-trail wind in the same manner that is used to obtain a balloon sounding, the usual averaging distance being about 2,000 feet. Large discrepancies between the two soundings are noted, particularly at 17,000 feet.

On a digital computer, a Scout launch vehicle was "flown" through these two winds, the results of which are shown in figure 15. Shown is an envelope of the bending moment plotted against altitude for the smoke trail and simulated balloon inputs. Note, in particular, the large difference in loading at an altitude of about 17,000 feet. Most of this difference can be ascribed to dynamic effects of flying through this detailed wind velocity as given by the smoke trail. In the insert is shown the actual bending-moment trace and again the large dynamic effect is noted. Thus, it is apparent that more detailed and realistic wind profiles are needed for proper design.

With regard to providing information for operational purposes, the smoke-trail procedure requires too much time for data reduction. However, the U.S. Air Force Cambridge Research Laboratory has under development a so-called "super pressure balloon" which, when used with a much more accurate radar system, could provide this operational information.

#### CONCLUDING REMARKS

This discussion has pointed up a number of structural dynamic areas that will require detailed investigation when the final configuration is selected. In particular, the vibration characteristics of the Apollo on the Saturn launch vehicle should be determined, perhaps by a dynamic model, and the need for a very thorough buffet investigation is indicated. Of course, research efforts to advance the state of the art must proceed hand

03:17:00 [REDACTED] 03:00

in hand with these more specific items to provide a reliable basis for design procedures and prediction of loads associated with launch-vehicle dynamics.

Langley Research Center,  
National Aeronautics and Space Administration,  
Langley Air Force Base, Va., July 18, 1961.

#### REFERENCES

1. Coe, Charles F.: Steady and Fluctuating Pressures at Transonic Speeds on Two Space-Vehicle Payload Shapes. NASA TM X-503, 1961.
2. Henry, Robert M., Brandon, George W., Tolefson, Harold B., and Lanford, Wade E.: The Smoke-Trail Method for Obtaining Detailed Measurements of the Vertical Wind Profile for Application to Missile-Dynamic-Response Problems. NASA TN D-976, 1961.

L  
1  
7  
5  
5

[REDACTED]

CONFIDENTIAL

11

## LOADING CONDITIONS DURING FLIGHT

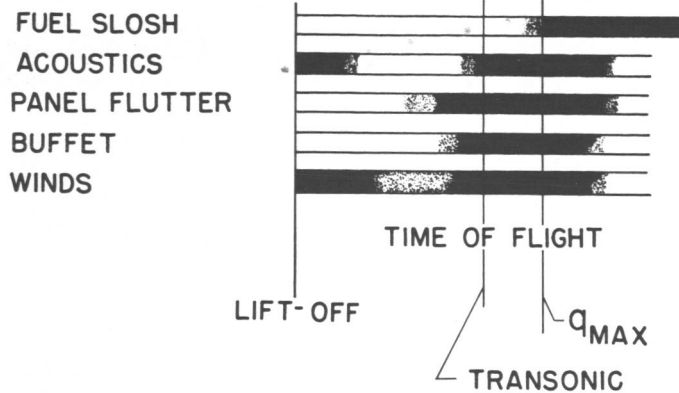


Figure 1

## SATURN VIBRATION MODEL

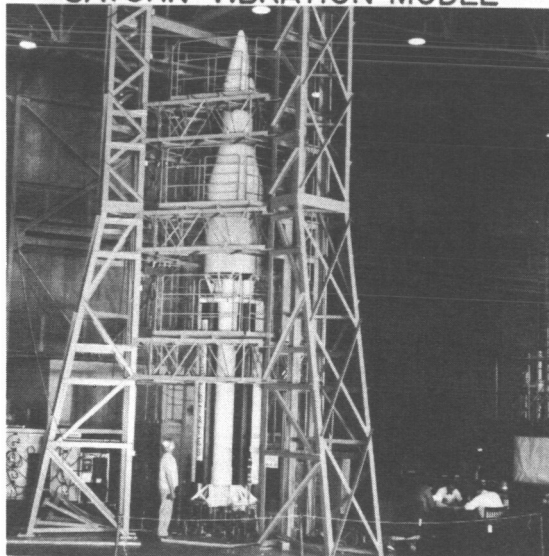


Figure 2

L-61-3024

CONFIDENTIAL

L-1755

0347030

## FREQUENCY RESPONSE OF SATURN MODEL

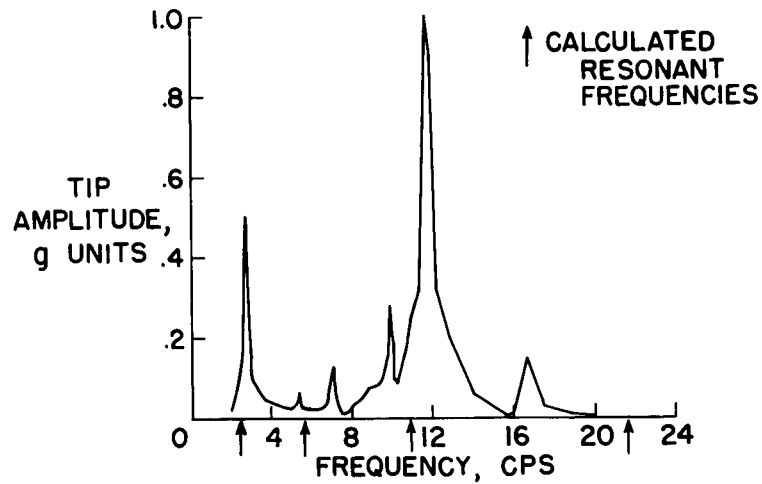


Figure 3

## FIRST VIBRATION MODE

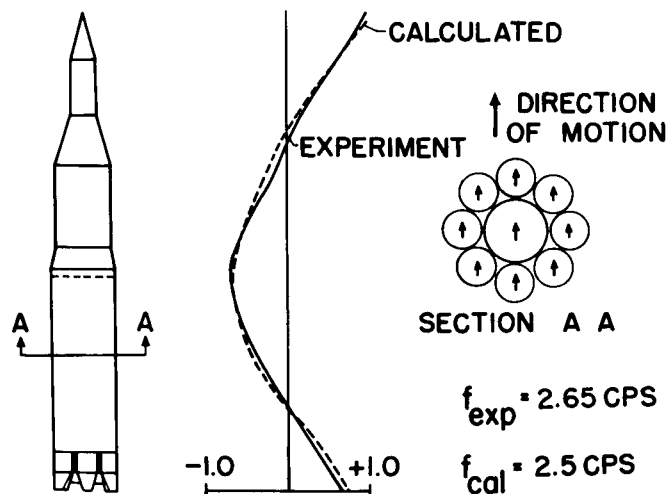


Figure 4

~~CONFIDENTIAL~~

## SECOND VIBRATION MODE

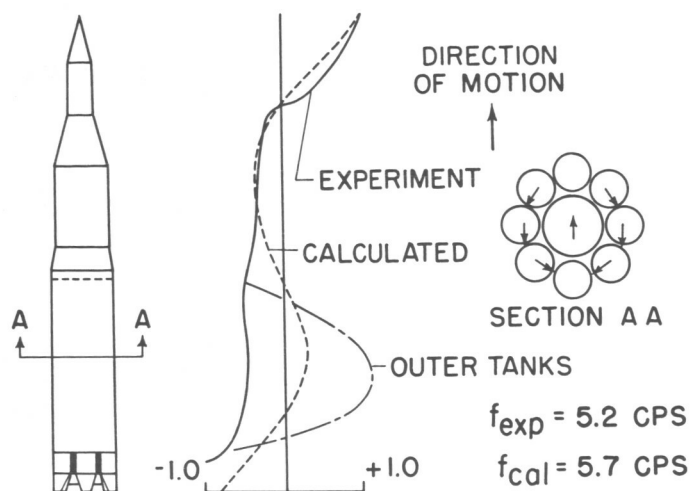


Figure 5

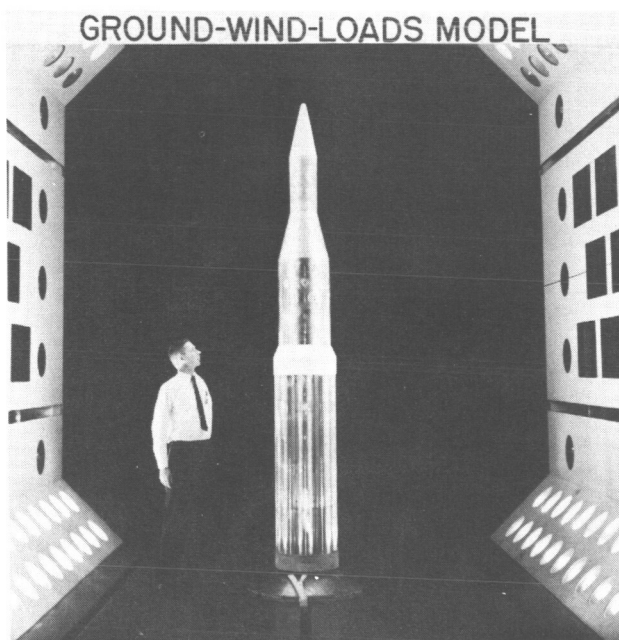


Figure 6

L-61-1628

~~CONFIDENTIAL~~

0317: [REDACTED] 030

## SATURN GROUND-WIND INDUCED LOADS

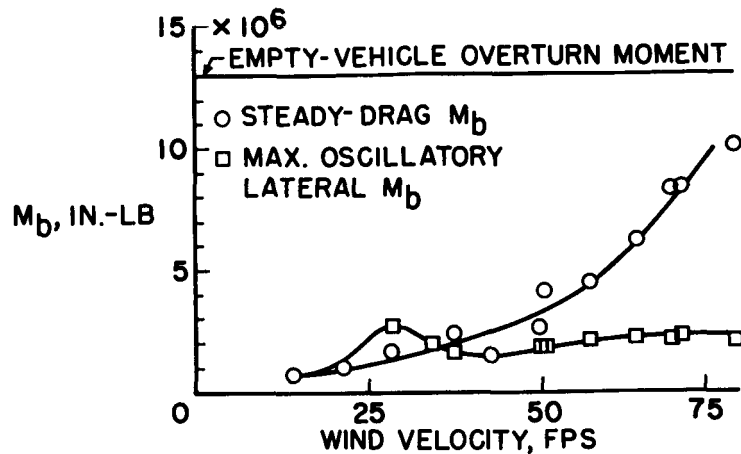


Figure 7

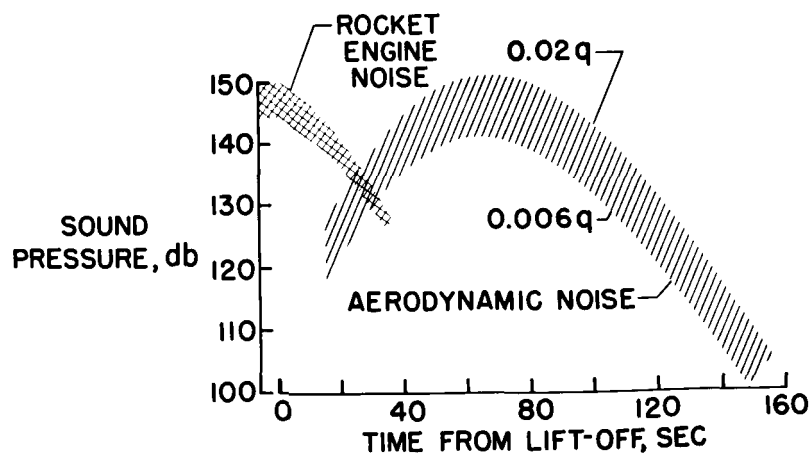
ESTIMATED EXTERNAL ACOUSTIC ENVIRONMENT  
OF MANNED SPACECRAFT

Figure 8

# SOME CONFIGURATIONS STUDIED IN NASA BUFFET PROGRAM

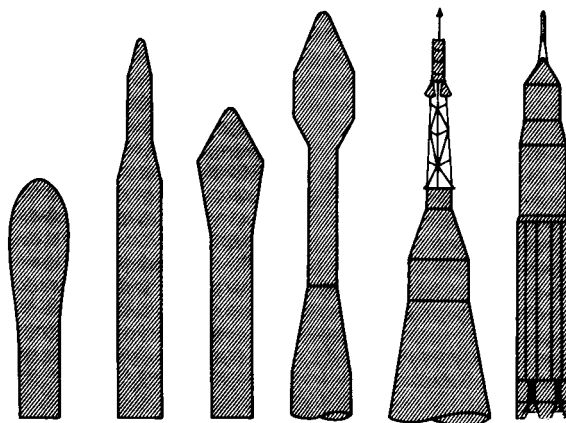
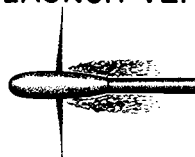


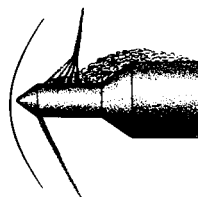
Figure 9

## TYPES OF BUFFET FLOWS ON LAUNCH VEHICLES

I SHOCK-BOUNDARY  
LAYER INTERACTIONS



II UPSTREAM PRESSURE PROPAGATION



III WAKE BUFFET

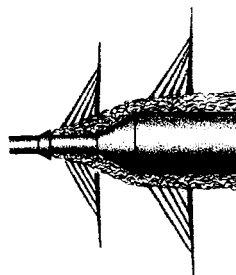


Figure 10

CONFIDENTIAL

### BUFFET PRESSURE DISTRIBUTION ON CONE CYLINDER

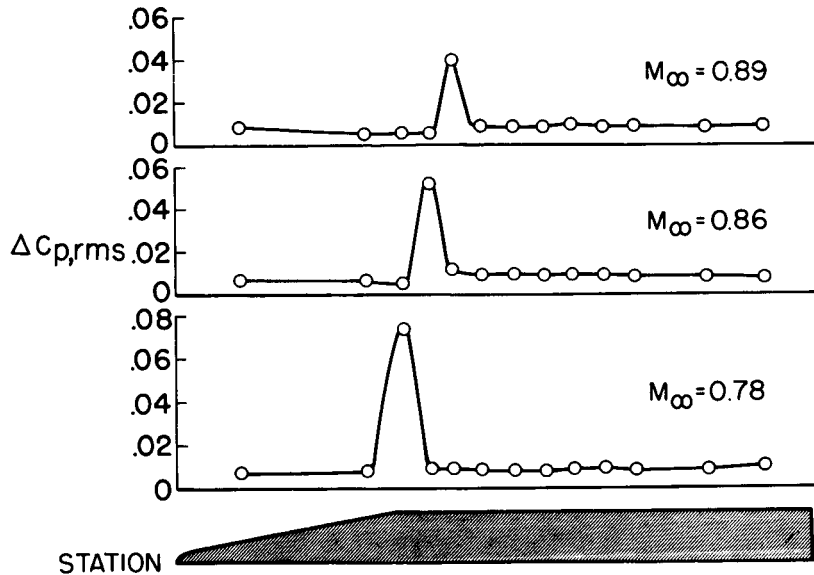


Figure 11

### EFFECT OF ESCAPE TOWER ON BUFFET LOADS

$M_\infty = 0.95$ ;  $\alpha = 0^\circ$

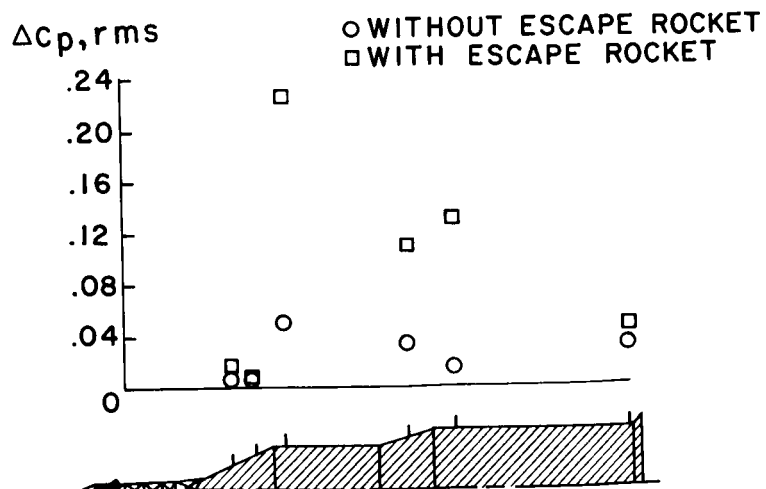


Figure 12

CONFIDENTIAL



DECLASSIFIED

EFFECT OF NOSE SHAPE ON AERODYNAMIC DAMPING OF FIRST ELASTIC MODE

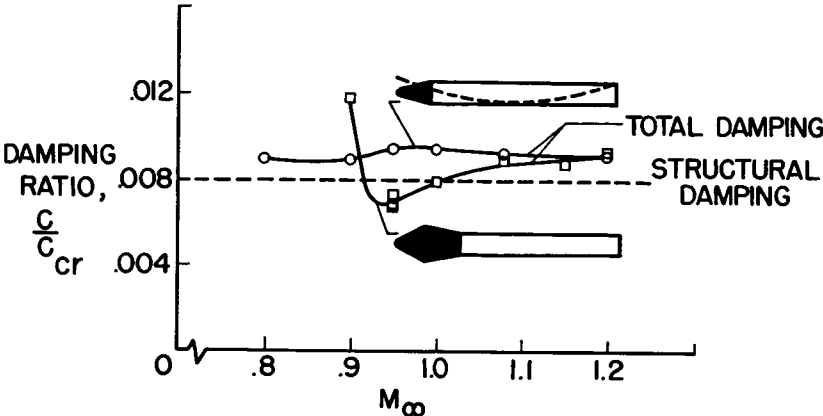


Figure 13

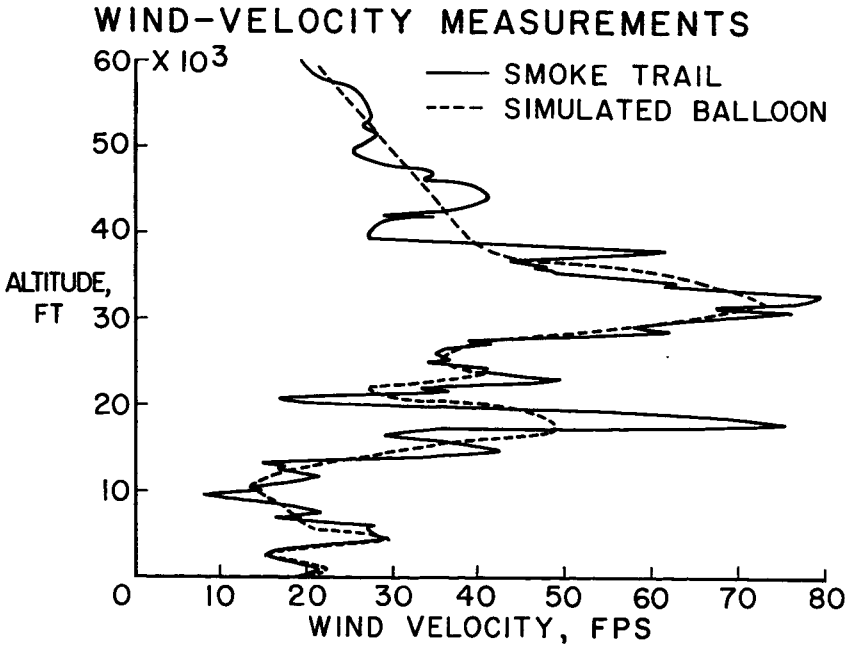


Figure 14

0371030

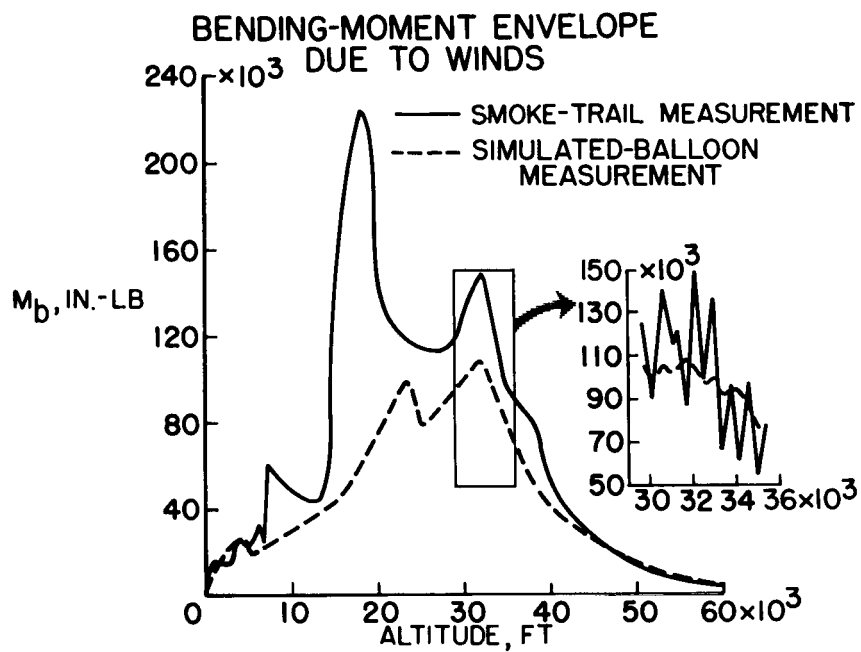


Figure 15